The Cryosphere Discuss., 8, 2831–2866, 2014
www.the-cryosphere-discuss.net/8/2831/2014/
doi:10.5194/tcd-8-2831-2014

The Cryosphere Discussions
Open Access

Thermal characteristics of permafrost in the steep alpine rock walls of the Aiguille du Midi (Mont Blanc Massif, 3842 m a.s.l.)

F. Magnin[1], P. Deline[1], L. Ravanel[1], J. Noetzli[2], and P. Pogliotti[3]

[1]EDYTEM Lab, Université de Savoie, CNRS, Le Bourget-du-Lac, France
[2]Glaciology and Geomorphodynamics Group, Department of Geography, University of Zurich, Zurich, Switzerland
[3]ARPA Valle d'Aosta, Saint-Christophe, Italy

Received: 11 March 2014 – Accepted: 8 May 2014 – Published: 4 June 2014

Correspondence to: F. Magnin (florence.magnin@univ-savoie.fr) and P. Deline (philip.deline@univ-savoie.fr)

Published by Copernicus Publications on behalf of the European Geosciences Union.

Abstract

Permafrost and related thermo-hydro-mechanical processes are regarded as crucial factors in rock wall stability in high alpine areas, but a lack of field measurements means that the characteristics of such locations and the processes to which they are subjected are poorly understood. To help remedy this situation, in 2005 work began to install a monitoring system at the Aiguille du Midi (3842 m a.s.l.). This paper presents temperature records from nine surface sensors (eight years of records) and three 10 m-deep boreholes (four years of records), installed at locations with different surface and bedrock characteristics. Annual and seasonal offsets between mean surface temperatures and air temperatures suggest that snow cover and slope aspect are also important factors governing bedrock surface temperatures in steep terrain. Snow-free sensors revealed additional effects of microtopography and micrometeorology. Active layer thicknesses ranged from < 2 m to nearly 6 m, depending on sun-exposure and interannual variations in atmospheric conditions. Warm and cold permafrost (about −1.5 °C to −4.5 °C at 10 m-depth) coexists within the Aiguille du Midi, resulting in high lateral heat fluxes. A temperature inflection associated with a fracture provided evidence of non-conductive processes, most notably cooling due to air ventilation and some intermittent and local warming. Our field data, the first to be obtained from an Alpine permafrost site where temperatures are below −4 °C, confirm the results of previous studies of permafrost in steep bedrock slopes and highlight the importance of factors such as snow cover and fracturing.

1 Introduction

The last few decades have seen an increase in rockfall activity from steep, high-altitude rock walls in the Mont Blanc Massif (Western European Alps) (Ravanel and Deline, 2010; Deline et al., 2012). Several studies of recent rock avalanches and rockfalls in mid-latitude alpine ranges have ascribed such increases to climate-related permafrost

TCD
8, 2831–2866, 2014

degradation (Deline, 2001; Gruber et al., 2004a; Huggel et al., 2005, 2008; Fischer et al., 2006; Allen et al., 2009; Ravanel et al., 2010, 2012; Deline et al., 2011). Rockfall magnitude and frequency are thought to be linked to the timing and depth of permafrost degradation, which can range from a seasonal deepening of the active layer to long-term, deep-seated warming in response to a climate signal (Gruber and Haeberli, 2007). Local warming of cold permafrost may be induced by advection and the related erosion of cleft ice (Hasler et al., 2011b), which may lead to unexpected bedrock failures. As Krautblatter et al. (2011) noted, before being able to predict permafrost-related hazards, it is first necessary to develop a better understanding of the thermo-hydro-mechanical processes involved, which means collecting rock temperature measurements and develop modeling strategies.

Measurement strategies and numerical experiments have been used to investigate the thermal conditions and characteristics of near-vertical and virtually snow-free alpine rock walls that are directly coupled with the atmosphere (Gruber et al., 2003, 2004b; Noetzli et al., 2007). Hasler et al. (2011a) suggested that, compared with snow-free, smooth rock faces, thin accumulations of snow on micro-reliefs and cleft ventilation may both cause deviations of 1 to 3 °C in permafrost temperatures compared with the smooth, snow-free rock wall model test case. These recent advances in the study of steep, alpine rock walls have helped build bridges between what is known about the general characteristics of permafrost, which are mostly controlled by topoclimatic factors, and processes related to the microtopography and internal structure of the rock mass, which may be significant in the short-term and in surface layers. However, a much larger corpus of field observations and monitoring data for a variety of bedrock conditions is needed in order to develop, calibrate, and evaluate modeling strategies.

As part of our research into geomorphic activity in the Mont Blanc Massif, in 2005 we started a long-term permafrost-monitoring program at the Aiguille du Midi (AdM). Located on the NW side of the massif (Fig. 1), the AdM is now the highest instrumented bedrock permafrost site in the European Alps. As such it complements other

TCD
8, 2831–2866, 2014

observation sites, for example, those within the Swiss Permafrost Monitoring Network (PERMOS).

The present paper describes the monitoring stations on the AdM and presents data from nine surface-temperature loggers and three 10 m-deep boreholes. We used these data to draw up a detailed description of the thermal regime at the AdM and to analyze the annual regime and seasonal variations in the surface thermal regime in the light of microtopographical settings and differences in snow cover. Four years of borehole data provided insights into active layer patterns, permafrost characteristics, and a fracture-induced temperature anomaly that stood out clearly in the calculated heat fluxes.

2 Study site

2.1 General setting

The summit of the AdM (45.88° N, 6.89° E) consists of three granite peaks (Piton Nord, Piton Central, and Piton Sud) and culminates at 3842 m a.s.l. (Fig. 2). The steep and partly glaciated north and west faces of the AdM tower more than 1000 m above the Glacier des Pélerins and Glacier des Bossons, while its south face rises just 250 m above the Glacier du Géant (i.e., the accumulation zone of the Mer de Glace). This part of the Mont Blanc Massif is formed by an inclusion-rich, porphyritic granite and is bounded by a wide shear zone. A main, N 40° E fault network intersected by a secondary network determines the distribution of the main granite spurs and gullies (Leloup et al., 2005). The highest parts of the peak tend to be steep, contain few large fractures, and, in places, are characterized by vertical foliation bands and small fissures. The lower parts are less steep and more fractured. In the present paper we use the abbreviation AdM to refer only to the upper section of the Piton Central, between 3740 and 3842 m a.s.l.

TCD
8, 2831–2866, 2014

A tourist cable car runs from Chamonix to the Piton Nord. Galleries and an elevator allow visitors to gain the viewing platform on top of the Piton Central, from where there is a 360° panorama of the Mont Blanc Massif.

2.2 Research context and strategies

We chose the AdM as a monitoring site for the following scientific and logistical reasons: (i) permafrost is extremely likely due to the AdM's high altitude and the presence of cold-based hanging glaciers on its north face; (ii) the morphology of the peak, which offers a range of aspects, slope angles, and fracture densities that are representative of many other rock walls in the massif; (iii) the easy access by cable-car from Chamonix and the availability of services (e.g., electricity) at the summit station.

Monitoring equipment was installed as part of the *PERMAdataROC* (2006–2008) and *PermaNET* (2008–2011) projects, funded by the European Union and run jointly by EDYTEM Lab (France), ARPA VdA (Italy), and the Universities of Zurich (Switzerland), Bonn, and Munich (Germany).

The monitoring program was designed to meet three scientific goals:

1. Characterize the surface temperatures of high-alpine, steep rock walls,
2. Determine the thermal state of the permafrost and analyze processes such as active-layer formation and permafrost changes at depth,
3. Obtain data that can be used for high-resolution modeling of permafrost distribution and thermal processes, taking into account the effects of snow cover and bedrock structure.

TCD
8, 2831–2866, 2014

3 Monitoring system

3.1 Rock temperature monitoring

Rock surface temperatures at the top of the AdM (between 3815 and 3825 m a.s.l.) have been monitored since 2005 using mini-loggers (GeoPrecision PT1000 sensors, accuracy ±0.1 °C) installed by the University of Zurich and ARPA VdA. Each face of the AdM has two loggers installed in snow free locations (Table 1). The south face has an additional logger (S3) installed just above a small ledge on which snow accumulates in winter, covering the logger. The loggers record the temperature every hour at depths of 0.03, 0.30, and 0.55 m, in line with the method described by Gruber et al. (2003).

In September 2009, three boreholes were drilled in the lower section of the Piton Central, at between 3738 and 3753 m a.s.l. In order to minimize possible thermal disturbances, the boreholes were drilled several tens of meters below the galleries running through the AdM, with the exact location of each borehole being chosen according to the aspect, fracturing, roughness, and angle of the rock wall (Fig. 2). Each borehole was drilled perpendicular to the rock surface and to a depth of 11 m. Borehole depths were constrained by the drilling equipment and the funding available. The boreholes on the northeast (BH_E) and south (BH_S) faces were drilled in fractured rock walls that slope at 65° and 55°, respectively. Even on rock walls at these angles, snow can accumulate on the micro-reliefs in the face. The borehole on the northwest face (BH_N) was drilled in a vertical, unfractured wall. The only place that snow can accumulate on this wall is on small ledges such as the one above which BH_N was drilled.

The boreholes were drilled between 14 September and 27 September 2009 by a team of five people (two mountain guides, plus three members of the EDYTEM Lab) who had to contend with very variable weather and challenging logistics. For each borehole it was necessary to: (i) install a safety line for the workers, (ii) set up a rope system to carry the equipment from the galleries to the drill site, (iii) install a work platform for the three drillers, (iv) anchor a base on which to fix a rack way, (v) drill the hole using a 380-V Weka Diamond-Core DK 22 electric drill, (vi) insert into the hole

TCD
8, 2831–2866, 2014

a polyethylene PE100 tube (outer diameter: 40 mm; inner diameter: 29 mm) sealed at its bottom, and (vii) remove the work platform. In addition to the difficult environment and harsh weather, the drilling work was complicated by the heterogeneity and hardness of the granite, which took a heavy toll on the equipment (11 diamond heads worn out or broken, a dozen steel tubes damaged, and a motor broken). At first we tried to drill 46 mm-diameter boreholes but we had to increase the diameter to 66 mm so we could use a more robust pipe string. Cooling required 1 to 3 m^3 of water per day, which was carried up from Chamonix in 1 m^3-tanks via the cable car.

The three boreholes were fitted with Stump 10 m-long thermistor chains, each with 15 nodes (YSI 44031 sensors, accuracy ±0.1 °C) arranged along a 6 mm fiberglass rod. Following calibration at 0 °C in an ice-water basin, the sensors were inserted in BH_S and BH_N in December 2009 and in BH_E in April 2010 (Fig. 3). In order to prevent heat convection, each sensor was separated from the others on the chain by insulating foam. The boreholes were closed at the top, but the chains can be removed to check for thermistor drift. Rock temperatures at depths between 0.3 and 10 m are recorded every three hours (Table 1). Because BH_S is shallower than 10 m, the thermistor chain protrudes from the rock surface by 36 cm. Temperature comparisons between BH_S and BH_N/BH_E were carried out at the closest equivalent depths (e.g., temperatures at a depth of 2.64 m in BH_S were compared with temperatures at a depth of 2.5 m in BH_E and BH_N).

3.2 Complementary permafrost measurements

Two automatic cameras take six pictures per day of the borehole sites on the south and northeast faces. Five graduated stakes were installed in January 2011 in various depths of snow to evaluate snow accumulation patterns on each face. During the winters of 2011 and 2012, thick snow (> 1 m) accumulated on the south face and lasted until late spring. The thickness of the snow on the northeast face (< 0.5 m) was more variable because the steepness and geometry of the face means that snow sloughs off quite rapidly after snowfall. BH_N is covered by a snow patch that is over 1 m thick for

TCD
8, 2831–2866, 2014

most of the year. RST_S3 is also frequently covered by > 0.5 m of snow during winter and spring.

In conjunction with the Universities of Bonn and Munich, four Electrical Resistivity Tomography (ERT) and Induced Polarization (IP) measurement campaigns have been carried out since 2008. Measurements were taken (i) on two horizontal transects along the galleries and rock walls of the Piton Central and Piton Nord, and (ii) on a vertical transect from the summit to the steep north and south faces of the Piton Central. ERT provides a 2-D cross section of a rock mass's resistivity. IP is used to measure the charge storage capacity of cracks filled with fine material.

Météo France has continuously monitored air temperature (AT, Table 1), wind speed, and wind direction at the top of the Piton Central since February 2007. Data prior to 2007 (1989–2006) are very fragmented due to insufficient equipment maintenance and are not used in this study.

From 2006 to 2010, ARPA VdA measured air temperature and relative humidity on the south and north faces, using mini-dataloggers inside radiation shields. In addition, an automatic weather station on the south face records incoming and outgoing shortwave and longwave solar radiation, wind speed, and wind direction every 10 min.

Finally, we calculated a high-resolution (cm-scale) triangulated irregular network (TIN) model of the AdM, using point clouds obtained by terrestrial laser scanning. The rock walls were scanned in December 2006 and in May and July 2008 using a long-range Optech ILRIS 3-D scanner, whereas the galleries were scanned in July 2008 and March 2009 using short-range FARO LS 880 and Leica HDS 6000 scanners.

4 Dataset preparation

The borehole time series are all continuous except for short periods for BH_S, as this logger was removed from September 2012 to January 2013 and from October 2013 to January 2014 to prevent it being damaged by engineering work close to the borehole. Gaps in the 0.3 m-deep temperature and AT time series were filled in so we could

TCD
8, 2831–2866, 2014

calculate seasonal and annual means (cf. Table 2). Short gaps (< 5 days) were filled by linear interpolation between the nearest available data points for the same depth; longer gaps (up to 1.5 months) were filled by replacing missing data with the average value for the 30 days before and 30 days after the gap (cf. Hasler et al., 2011a). To fill the longest gaps for E1, N1, S1, and W1 (from 4 December 2007 to 7 February 2008) we used a third approach that involved applying a linear regression equation, fitted using data from each pair of loggers (e.g., E2 and E1) and from the gap periods (i.e., December–February) for groups of years with complete records (2006–2007 and 2008–2009). Correlation coefficients for the equations ranged from 0.89 (S1 and S2) to 0.94 (E1 and E2). We tested this approach by simulating corresponding gap periods in the years with complete data and then filling these gaps using the regression equations. Differences between the annual means obtained using this method and the annual means calculated from the complete data set were in the range 0.01–0.15 °C and can be considered negligible. Our calculations of seasonal means did not include data obtained using the 30 day average or linear regression methods. We did not fill gaps longer than 1.5 months because we felt that the resulting data would not be reliable enough to give realistic annual means.

5 Rock surface temperature characteristics

Smith and Riseborough (2002) defined Surface Offset (SO) as the difference between local Mean Annual Air Temperature (MAAT) and Mean Annual Ground Surface Temperature (MAGST). Surface offset is a parameter in the TTOP model (Temperature at the Top of Permafrost, Smith and Riseborough, 1996), originally developed to define the functional relation between air and ground thermal regimes in polar lowlands and later applied to high-latitude mountainous terrain (Juliussen and Humlum, 2007). SO can be used to quantify the overall effect of ground cover and ground surface parameters on the surface energy balance. For steep, snow-free bedrock, temperature differences between the rock surface and the air are mainly due to direct solar radiation (Gruber

TCD
8, 2831–2866, 2014

et al., 2004b). In the European Alps, the MAGST for steep rock is usually higher than the MAAT, with an SO of up to 12 °C for south-facing rock walls. However, such high values are probably partly due to reflected solar radiation from large, bright glacier surfaces below measurement points (PERMOS, 2013). In Norway, maximum values for steep rock walls are only 3 °C (Hipp et al., 2014), as there is less direct solar radiation at these higher latitudes. Allen et al. (2009) reported a maximum value of 6.7 °C for New Zealand, which is at a similar latitude to the Alps. This is because the oceanic influence on the climate probably results in greater cloud cover, thereby reducing insolation.

Most surface sensors have been installed in snow-free conditions in order to test energy balance models (Gruber et al., 2004b) or for statistical fitting (Allen et al., 2009; Boeckli et al., 2012). Because the AdM dataset covers eight years and a variety of bedrock surface characteristics, it provides insight into the effects of variations in snow cover and into surface temperature trends. We calculated both annual SOs (ASO), using annual means, and seasonal SOs (SSO) for winter (December to February), spring (from March to May), summer (from June to August), and fall (from September to November), using time series measured at depths of 0.3 m (boreholes and E2, S2, W2, N2) and 0.1 m (E1, S1, W1, N1) – points we considered representative of surface conditions. Figure 4 shows ASOs for all the complete years (Fig. 4a), SSOs for snow-free sensors for the available seasons (Fig. 4b), and SSOs for snow-covered sensors for the available seasons (Fig. 4c). The pattern of snow accumulation and its effects are discussed in relation to daily temperature variations (Fig. 5).

5.1 Annual surface offset patterns

Maximum and minimum ASOs were 9.5 °C, recorded at S1 in 2011, and 1.5 °C, recorded at N1 in 2009 (Fig. 4a). These are typical values for the European Alps (see PERMOS, 2013). On the south face, the snow-covered sensors gave lower values than the snow-free sensors. For example, the ASOs for S3 (no. 6) were between 0.1 °C (2010) and 1.4 °C (2011) lower than the ASOs for S1 (no. 5). This is due to the high albedo of the snow that covers the sensor for a significant part of the year. Conversely,

TCD
8, 2831–2866, 2014

on the north side, the snow-covered sensor gave higher ASOs than the snow-free sensors, probably due to the snow insulating the sensors from the cold. However, this interpretation does not take into account the fact that BH_N (no. 11) and the snow-free sensors (no. 10 and 11) were in different topographical settings (100 m altitude difference, microtopography).

Although the influence of snow cover on BH_E (no. 1) is difficult to determine because there is no snow-free sensor in similar conditions, the interannual variability at BH_E between 2011 and 2012 was high (+1.1 °C). A similarly high interannual variability was recorded at BH_N but not by the snow-free sensors. The interannual variability of the snow-covered sensors depended mainly on the depth and duration of the snow cover and was therefore greater than the interannual variability at the snow-free sensor. These results show that interannual variabilities can differ between different parts of a rock wall, thereby complementing the PERMOS reports (2013), which showed differences in interannual variability between rock walls and less-steep, snow-covered terrain. However, at the snow-covered, south-facing S3 sensor, the 2011–2012 interannual variability was much lower (+0.3 °C) than it was at the other snow-covered sensors. Conversely to the snow-covered sensors, the 2011–2012 variability recorded by the snow-free sensors was negative, with, for example, values of −1 °C at S2 and −0.3 °C at E1. The interannual variability of snow-free sensors is mainly related to differences in insolation due to clouds. Consequently, the temperature at a snow-covered sensor can increase from one year to the next if increased snowfall insulates the sensor from the atmospheric temperature, whereas the temperature at a snow-free sensor may drop due to reduced insolation. The effect of snow-cover is greater on sensors in the shade and the effect of reduced insolation is greater on sensors on sunny faces. Sensors that are both snow covered and exposed to the sun, such as S3 (no. 6), would combine warming due to snow insulation and cooling due to snow having a higher albedo than rock. As a result, interannual temperature variability will be smaller at these sensors than at sensors in shadier locations, where the variability is mostly due to variations in snow cover. The maximum and minimum ASOs for the different snow-free

TCD
8, 2831–2866, 2014

sensors did not occur in the same years. For example, the maximum ASOs at W1 and W2 (no. 8 and 9) occurred in 2008, but in 2011 at S1 and S2 (no. 5 and 7). This is interpreted as being due to variations in cloud formation from year to year, thus highlighting the effect of micrometeorology on the surface thermal regime.

The ASOs show that, compared with the snow-free sensors, surface temperatures were lower at the sun-exposed and snow-covered sensors and higher at the shady sensors. Interannual variability for 2011–2012 was negative at the snow-free sensors but positive at the snow-covered sensors. The snow-covered, shady sensors recorded the highest interannual variabilities. Interannual variabilities at the snow-free sensors were consistent with their aspect. These findings show that the effects of snow cover and micrometeorology can differ greatly between different aspects.

5.2 Seasonal surface offset patterns

For the snow-free sensors (Fig. 4b), maximum SSOs occurred in summer, except for the sensors on the south face (no. 5 and 7), where the maximum SSOs occurred in spring, with values > 10 °C. The lowest SSOs were recorded in winter, and ranged from approximately 8 °C on the south face to < 1 °C on the north face (no. 12 and 10). These patterns are controlled by the duration of insolation and reveal a possible influence of rock wall slope, as the high spring SOs on the south face were probably due to the sun's rays being more perpendicular to the sub-vertical face.

SSO patterns for the snow-covered sensors (Fig. 4c) were opposite to those for the snow-free sensors. At BH_N and BH_S (no. 11 and 4), SSOs were largest in winter (4.8 °C and 10 °C, respectively), thereby confirming the insulating effect of snow. SSOs were lowest in summer, suggesting that the sensors remained covered in snow, and therefore protected from the sun, for a substantial part of the summer. Similarly, the high autumn SSO at BH_N was probably due to early season snowfall. The SSO pattern at BH_E suggests that duration of insolation was the main controlling factor and that snow cover had a limited effect.

TCD
8, 2831–2866, 2014

These SSOs show that temperatures were higher at the snow-covered sensors than at the snow-free sensors in winter, and lower at the snow-covered sensors than at the snow-free sensors in summer. In summer snow cover has a "cooling effect" by increasing the albedo compared with bare bedrock, whereas in winter it has a "warming effect" by insulating the rock from the cold air. On the sunny south face, the summer cooling effect is stronger than the winter warming effect, so it is the summer cooling effect that dominates the annual surface offset. Conversely, on the shady north face, the winter warming effect is stronger than the summer cooling effect, so the dominant factor is the winter warming effect. The SOs at the snow-covered BH_E sensor were more consistent with insolation parameters, which suggests that the snow cover here has different effects. The SOs for the snow-free sensors also highlight the effect of slope angle on the strength of solar radiation.

5.3 Thermal regime of snow-covered sensors

Temperature curves during the cold period were smoother than the expected daily oscillations, with the length and amplitude of the residual oscillations depending on the sensor (Fig. 5). The S3 and BH_S temperature curves were smoothed from mid-November 2010 to January (BH_S) or April 2011 (gap for S3), and from early December 2011 to mid-May 2012. Both sensors recorded a period of almost isothermal conditions from April to mid-May 2012, probably due to the zero-curtain effect (i.e., latent heat from phase changes during spring snow melt). A similar phenomenon has been reported for seasonally snow-covered, gentle mountain slopes (e.g. Hanson and Hoelzle, 2004; Gubler et al., 2011). The temperature curve for BH_N was smoothed until the summer, with a three-week zero-curtain effect in July 2011. Due to year-to-year weather variations, the zero-curtain effect did not occur at every location every year and did not occur year-after-year at the same location.

Although the BH_E temperature curve from late September to February–March was mostly smoother than the expected daily oscillations, it was more closely coupled to AT than the curves for the other sensors, as it oscillated in-synch with major changes in AT,

TCD
8, 2831–2866, 2014

such as the large drop in temperature in December 2012. The temperatures recorded at BH_E were lower than those recorded at BH_N during certain periods (September 2010 to March 2011, November 2011 to February 2012). This could be the result of (i) the contrast between the greater insulating effect of the thick snow on the terrace where BH_N is located (the temperature curve for BH_N during periods of snow cover is much smoother than the curves for the other sensors); (ii) the poor insulating effect of the thin and intermittent snow cover over BH_E. These differences are in line with data obtained from gentler mountain slopes (Hanson and Hoelzle, 2004) and numerical experiments (Luetschg et al., 2008; Pogliotti, 2011), which define an insulating threshold of 0.6–0.8 m as the boundary between the cooling and warming effect of snow.

Daily records confirmed the insulating effect of thick snow deposits and showed that melting can last several weeks, as is the case on gentle mountain slopes with seasonal snow cover; although, snow cover can subsist until late summer at high altitudes. Also in accordance with previous studies, thin snow cover probably had an overall cooling effect.

6 Borehole records

Four years of data from the three boreholes allowed us to describe the thermal regime in terms of daily temperature profiles (Fig. 6), mean annual Temperature–Depth ($T(z)$) profiles, and annual temperature envelopes (i.e., the maximum and minimum temperatures at each depth; Fig. 7). We focused on the active layer and the permafrost conditions, paying special attention to thermal effects related to bedrock structure.

6.1 Active layer

Active Layer Thickness (ALT) varied with aspect, with means of ca. 3 m at BH_E, 5.5 m at BH_S, and 2.2 m at BH_N (Fig. 6). Interannual variability during the monitoring period was ca. 0.7 m for each borehole (Table 3). This variability is consistent

TCD
8, 2831–2866, 2014

with interannual variability values reported for Swiss boreholes in bedrock, which are usually higher than those for debris slopes (e.g., Matterhorn or Schilthorn compared with Flüela or Muragl, PERMOS 2010, 2013). Further comparisons with Swiss data are difficult because of the specific characteristics of the AdM. As Table 3 shows, the maximum ALT for each borehole occurred in 2012 for BH_N (2.5 m deep), in 2013 for BH_E (3.4 m deep), and in 2011 for BH_S (5.9 m deep; however, there are no relevant data for 2012). The interannual variability between the boreholes suggests differences in heat transport, probably due to differences in rock structure and related air/water circulation, as well as to ice content. This hypothesis is discussed further in the following section. In addition, summer snowfall may have contributed to reducing the thickness of the BH_E active layer in 2011.

The length of the thawing period, marked by continuous positive temperatures at the uppermost thermistor, also varies according to aspect. It is longest at BH_S, starting in June (April in 2011), but with isolated thawing days already in March (e.g., in 2012). In general, the surface refroze in October but total refreezing of the active layer did not occur until December in 2010 and 2011. The 2011–2012 freezing period was particularly mild and short (3–4 months) at BH_S. This pattern was not as marked at BH_E, which even recorded its lowest surface temperature in 2011–2012. The relatively mild and short 2011–2012 freezing period at BH_S may be the result of snow insulation, as is suggested by the subsequent period of isothermal conditions from the surface to a depth of 3 m, which may be due to latent heat effects (see Sect. 5.3). BH_N had the longest freezing periods because temperatures in the rock sub-surface remained positive only from June to October. In 2011, thawing did not start until August. BH_E had the most balanced thawing and freezing periods (ca. 6 months each).

The timing of maximum ALT depended on aspect and year (Table 3). In 2010 and 2011, maximum ALT occurred earliest at BH_E, even though the active layer was thicker at BH_E than at BH_N. In 2012 and 2013, BH_N was the first site to reach maximum ALT. In 2010, maximum ALT at BH_S occurred very late, three months later than at BH_E. Although the BH_S active layer had mostly thawed by mid-July, thawing

TCD
8, 2831–2866, 2014

continued steadily until the end of October. Maximum ALT always occurred later at BH_S than at the other boreholes, but the lowering of the 0 °C isotherm was more linear. ALT at BH_S may be influenced by phase-change processes delaying thawing and refreezing. This is consistent with the range of interannual variability at BH_S, which was not much greater than at BH_N, for example, from 2010 to 2011 (Table 3), although interannual variability tends to be greater for sunny faces than for shady faces (Gruber et al., 2004a). The presence of wet detritic material in bedrock discontinuities, noted during drilling, supports these assumptions about the effects of phase-change processes.

At the AdM, active layer thicknesses and the timing of maximum ALT are mostly governed by topoclimatic factors. However, snow cover may also affect the interannual variability between boreholes, the timing of the thawing season, and the intensity of freezing. In addition, the active layer freezing and thawing pattern at the south-facing borehole may have been influenced by phase change processes, as the late refreezing and interannual variability were similar to those at the shady boreholes.

6.2 Thermal regime

Annual Temperature–Depth $T(z)$ profiles (Fig. 7a) revealed different thermal regimes. The AdM's Piton Central has both warm (ca. −1.5 °C at BH_S) and cold (ca. −4.5 °C at BH_N) permafrost (Table 3). The zero annual amplitude depth is > 10 m (Fig. 7b), which is consistent with other bedrock sites in the European Alps (PERMOS, 2007). In 2011, the largest amplitudes at the surface (> 20 °C) and at 10 m depth (1.6 °C) were at BH_E, and the smallest surface (15.5 °C) and 10 m (1.0 °C) amplitudes were at BH_N and BH_S. In line with the surface pattern, the minimum $T(z)$ profile from the surface to 1.4 m deep was warmer at BH_N than at the sunnier BH_E (Fig. 7b), suggesting that this layer is affected by snow insulation.

The minimum and mean annual $T(z)$ profiles for BH_N contain two distinct sections separated by an inflection at ca. 2.5 m deep (Fig. 7a). This coincides with an 8–10 cm-wide cleft encountered at this depth during the drilling operation. The temperature

TCD
8, 2831–2866, 2014

gradient is negative ($-0.39\,^{\circ}\mathrm{C\,m^{-1}}$) from the surface to the cleft, and then positive from the cleft to 10 m-deep (from $0.16\,^{\circ}\mathrm{C\,m^{-1}}$ to nearly isothermal). The mean annual profiles for BH_E are almost linear and have a temperature gradient of ca. $-0.2\,^{\circ}\mathrm{C\,m^{-1}}$. Small inflections in the profiles (e.g., at 1.1 m, 2.5 m, and 7 m depth) occur every year, suggesting that they are due to the structure of the bedrock. The linearity of the BH_E profiles indicates that the most important process is heat conduction (Williams and Smith, 1989), whereas the inflections in the BH_N profiles are the result of non-conductive processes at the cleft. In the case of BH_S, the upper parts of the annual $T(z)$ profiles for 2010 and 2011 differ greatly, with an almost linear temperature gradient of $-0.07\,^{\circ}\mathrm{C\ m^{-1}}$ in 2010, and a much steeper overall temperature gradient of $-2.26\,^{\circ}\mathrm{C\,m^{-1}}$ in 2011. The shallowest 6 m were warmer in 2011 than in 2010, with positive temperatures to a depth of 1 m. The temperature at greater depths was almost constant during both years, although it was slightly lower in 2011 than in 2010. As for the active layer pattern, the shape of the BH_S profile and the reduced inter-annual thermal change at depth may be the result of phase-change processes due to water delaying and dampening the signal. The temperature gradient was negative (ca. $-0.1\,^{\circ}\mathrm{C\,m^{-1}}$) at the bottom of both profiles, in contrast to the positive gradient at the bottom of the BH_N profile. This feature is consistent with numerical simulations showing the role played by lateral heat flux from warm to cold faces in the thermal regime of alpine peaks (Noetzli et al., 2007), and confirms recent simulations of rock temperature distribution in a cross-section through the AdM (Noetzli et al., 2014).

These results confirm that temperature profiles are mostly controlled by topoclimatic factors; however, they also highlight the thermal effects of fractures (cooling in the BH_N profiles), and again suggest that the BH_S profiles may be influenced by phase-change processes. The negative $T(z)$ gradient in BH_S is probably the result of strong lateral heat flux towards the colder, north face. The upper parts of the BH_N profiles may reflect snow-cover effects but the presence of fracture effects makes it impossible to determine the respective contributions of these two factors from temperature data alone.

TCD
8, 2831–2866, 2014

6.3 Heat flux and bedrock structure

In a recent study of heat-exchange processes in bedrock discontinuities, Hasler et al. (2011b) noted that these processes may not be detectable through rock temperature records. However, the inflection in the temperature profile for the deep part of the BH_N $T(z)$ profile indicated the presence of a fracture, thereby showing that non-conductive heat transport can make a clear imprint on temperature records. In order to further investigate the heat transport processes associated with this fracture we calculated heat fluxes between each sensor depth (z) by solving the equation for vertical conductive heat flow (Qg, W m^{-2}) for each time step (Williams and Smith, 1989) in the daily temperature records (T):

$$\mathrm{Qg} = -K \times \frac{\partial T}{\partial z} \quad (1)$$

where K is thermal conductivity, taken to be 2.7 W m^{-1} K^{-1} in line with standard published values for granitic rock (Pogliotti et al., 2009; Cermak and Ryback, 1982).

As expected, the highest positive heat fluxes initiated at the surface occurred at BH_S during warm periods and the largest negative heat fluxes towards the surface occurred at BH_E during cold periods (Fig. 8). However, significant negative fluxes, initiated at the fracture depth, occurred between ca. 2.5 and 4 m depth at BH_N during cold periods. Significant heat inputs occurred immediately above these losses during warm periods. These heat inputs sometimes reinforced the heat flow from the surface, but most of the time they were disconnected from the surface signal. Energy inputs also occurred intermittently during the first months of the cold periods. These features suggest non-conductive heat transfer and are in line with observations made by Hasler et al. (2011a, b). The fracture acts as a thermal shortcut between the surface layer and the internal bedrock, constituting an additional boundary from which heat is transported. The dominant cooling effect, observed from the temperature records (see Sect. 6.2), may indicate air ventilation (Hasler et al., 2011a) through bedrock discontinuities, leading to globally colder conditions than would be expected if only conduction

TCD
8, 2831–2866, 2014

and surface temperature are taken into account. Finally, the localized warming is coherent with water percolating from the surface into clefts and warming the surrounding rock (Hasler et al., 2011b). However, why these two processes occur at different depths remains an open question. The small inflections in the BH_E mean annual profiles (Fig. 7) are also visible in the heat fluxes, especially at a depth of 2.5 m, where there is evidence of localized heat inputs, for example, from June to September 2012, but these inflections have a negligible impact on the overall pattern. The fracture width is probably the critical factor controlling the amplitude of the inflection by non-conductive processes.

Without the fracture inflection, heat fluxes in BH_N would be significantly reduced, especially heat losses, which were almost zero and relatively constant from the surface to the inflection depth (e.g. January–April 2010, January–February 2011, January–March 2012). Low but constant heat losses also occurred in the upper part of BH_S (especially during the 2012 and 2013 cold periods). In contrast, losses at BH_E were greater and changed more frequently. This is further evidence of the effect of snow insulation at BH_S and BH_N and the resulting reduced freezing of the active layer, and of a possible cooling effect of the thin snow cover over BH_E. In April–May 2012 an unusual heat gain occurred in all the boreholes. This heat gain penetrated from the surface to 3 m in BH_E and from the surface to 2 m in BH_N, and connected with a deep heat gain in BH_S at a depth of 10 m. It coincides with the zero curtain effect that occurred at the surface of BH_S in 2012 but it is probably climate driven because it occurred in all the boreholes at the same time.

Daily heat fluxes provide a better picture of the thermal characteristics of discontinuities than temperature records. The features surrounding the BH_N fracture suggest non-conductive heat transfer, probably due to ventilating air significantly cooling the rock from the fracture boundary downward, and to percolating water more locally and more intermittently warming the surrounding rock. The effects of snow insulation are also enhanced but further data are needed to evaluate the extent of this enhancement. However, the thermal features of BH_N show that the fracture has a greater impact

TCD
8, 2831–2866, 2014

than snow insulation on the permafrost thermal regime, whereas it seems that snow insulation has probably more influence on the active layer pattern.

7 Conclusions

The AdM's high altitude, peak morphology, and accessibility make it an exceptional site for investigating steep alpine bedrock permafrost. The monitoring equipment installed on the AdM has provided eight years of surface temperature data and four years of sub-surface temperature data for depths of up to 10 m and for rock walls with a variety of aspects and bedrock characteristics. The following conclusions can be drawn from the preliminary analysis of this new data:

1. The thermal characteristics of the AdM's rock walls are typical of steep bedrock permafrost. The topography controls the spatial distribution of surface temperatures, active layer thickness and timing, and the permafrost temperature regime.
2. These monitoring data confirm characteristics predicted by numerical experiments, including the coexistence within a single rock peak of warm and cold permafrost, which generates lateral heat fluxes from warm to cold faces.
3. Variable interannual differences between different aspects, and the range of SSOs, which are more consistent with the slope angle than with the length of insolation on the south face, suggest that surface temperature regimes in snow-free bedrock are partly governed by microtopographical and micrometeorological factors.
4. Interannual changes were greater for snow-covered locations and the trend of these changes may be opposite to that for snow-free locations (positive vs. negative interannual change).
5. The effect of snow cover on steep alpine faces is highly variable. Our results suggest that this effect is mostly related to snow depth and insolation:

TCD
8, 2831–2866, 2014

- Data from the sensor under thin snow cover was more consistent with insolation parameters, and temperatures were possibly lower than they would have been under snow-free conditions. In contrast, the three sensors under thicker snow cover show evidence of thermo-insulation.
- On the south face, the MAGSTs at the sensors under insulating snow accumulations were lower than those at the sensors in snow-free areas. Conversely, on the shady faces, the MAGSTs at the sensors under insulating snow accumulations were higher than those at the sensors in snow-free areas.
- The intensity of active layer freezing was probably reduced and active layer thawing may have been delayed in boreholes under thick snow cover; however, this was not the case every year, so it was probably related to weather conditions.

6. Some temperature data were affected by non-conductive processes related to bedrock structure:
   - Open fractures led to an overall cooling of the mean annual thermal profile at depth; however, this global effect is probably a combination of (i) the heat losses caused by ventilating air during the cold season, and (ii) local and intermittent heat gains during the warm season, possibly due to water percolating from the surface into the fracture.
   - The active layer depth and permafrost pattern of the AdM south borehole may have been affected by phase-change processes that delayed thawing and freezing, and dampened heat transfer at depth.

Our AdM dataset confirms a number of results obtained from measurements and numerical simulations of steep alpine rock walls. In addition, it provides further insights into the effects of variations in snow cover and bedrock structure. Further research is needed to quantify these effects.

TCD
8, 2831–2866, 2014

Acknowledgements. We acknowledge S. Gruber, U. Morra di Cella, E. Cremonese and E. Malet for their participation in installation and data acquisition at the Aiguille du Midi, as well as the *Compagnie des Guides* of Chamonix for their help in the drilling operations, the *Compagnie du Mont Blanc* (especially E. Desvaux) for the access at the site, and Météo France for the air temperature data. We thank P. Henderson for improving the quality of the English language. This work is supported by the Region Rhône-Alpes (*CIBLE* program).

References

Allen, S. K., Gruber, S., and Owens, I. F.: Exploring steep bedrock permafrost and its relationship with recent slope failures in the Southern Alps of New Zealand, Permafrost Periglac., 20, 345–356, doi:10.1002/ppp.658, 2009.

Boeckli, L., Brenning, A., Gruber, S., and Noetzli, J.: Permafrost distribution in the European Alps: calculation and evaluation of an index map and summary statistics, The Cryosphere, 6, 807–820, doi:10.5194/tc-6-807-2012, 2012.

Cermak, V. and Rybach, L.: Thermal conductivity and specific heat of minerals and rocks, in: Landolt–Börnstein Zahlenwerte and Funktionen aus Naturwissenschaften und Technik, Neue Serie, Physikalische Eigenschaften der Gesteine (V/1a), edited by: Angeneister, G., Springer, Berlin, 305–343. 1982.

Deline P.: Recent Brenva rock avalanches (Valley of Aosta): new chapter in an old story?, Geogr. Fis. Din. Quat., 5, 55–63, 2001.

Deline, P., Alberto, W., Broccolato, M., Hungr, O., Noetzli, J., Ravanel, L., and Tamburini, A.: The December 2008 Crammont rock avalanche, Mont Blanc massif area, Italy, Nat. Hazards Earth Syst. Sci., 11, 3307–3318, doi:10.5194/nhess-11-3307-2011, 2011.

Deline, P., Gardent, M., Magnin F., and Ravanel, L.: The morphodynamics of the Mont Blanc massif in a changing cryosphere: a comprehensive review, Geogr. Ann. A, 94, 265–283, 2012.

Fischer, L., Kääb, A., Huggel, C., and Noetzli, J.: Geology, glacier retreat and permafrost degradation as controlling factors of slope instabilities in a high-mountain rock wall: the Monte Rosa east face, Nat. Hazards Earth Syst. Sci., 6, 761–772, doi:10.5194/nhess-6-761-2006, 2006.

TCD
8, 2831–2866, 2014

Gruber, S. and Haeberli, W.: Permafrost in steep bedrock slopes and its temperature related destabilization following climate change, J. Geophys. Res., 112, F02S13, doi:10.1029/2006JF000547, 2007.
Gruber, S., Peter, M., Hoelzle, M., Woodhatch, I., and Haeberli. W.: Surface temperatures in steep alpine rock faces: a strategy for regional-scale measurement and modelling, in: Proceedings of 8th International Conference on Permafrost, Zürich, Taylor and Francis, Philadelphia, 325–330, 2003.
Gruber, S., Hoelzle, M., and Haeberli, W.: Permafrost thaw and destabilization of Alpine rock walls in the hot summer of 2003, Geophys. Res. Lett., 31, L13504, doi:10.1029/2004GL0250051, 2004a.
Gruber, S., Hoelzle, M., and Haeberli, W.: Rock-wall temperatures in the Alps: modelling their topographic distribution and regional differences, Permafrost Periglac., 15, 299–307, doi:10.1002/ppp.501, 2004b.
Gubler, S., Fiddes, J., Keller, M., and Gruber, S.: Scale-dependent measurement and analysis of ground surface temperature variability in alpine terrain, The Cryosphere, 5, 431–443, doi:10.5194/tc-5-431-2011, 2011.
Hanson, S. and Hoelzle, M.: The thermal regime of the active layer at the Murtèl rock glacier based on data from 2002, Permafrost Periglac., 15, 273–282, doi:10.1002/ppp.499, 2004.
Hasler, A., Gruber, S., and Haeberli, W.: Temperature variability and offset in steep alpine rock and ice faces, The Cryosphere, 5, 977–988, doi:10.5194/tc-5-977-2011, 2011a.
Hasler, A., Gruber, S., Font, M., and Dubois, A.: Advective heat transport in frozen rock clefts – conceptual model, laboratory experiments and numerical simulation, Permafrost Periglac., 22, 378–349, doi:10.1002/ppp.737, 2011b.
Hipp, T., Etzelmüller, B., and Westermann, S.: Permafrost in Alpine Rock Faces from Jotunheimen and Hurrungane, Southern Norway, Permafrost Periglac., 25, 1–13, doi:10.1002/ppp.1799, 2014.
Huggel, C., Zgraggen-Oswald, S., Haeberli, W., Kääb, A., Polkvoj, A., Galushkin, I., and Evans, S. G.: The 2002 rock/ice avalanche at Kolka/Karmadon, Russian Caucasus: assessment of extraordinary avalanche formation and mobility, and application of QuickBird satellite imagery, Nat. Hazards Earth Syst. Sci., 5, 173–187, doi:10.5194/nhess-5-173-2005, 2005.
Huggel, C., Caplan-Auerbach, J., and Wessels, R.: Recent extreme avalanches triggered by climate change, EOS T. Am. Geophys. Un., 89, 469–470, 2008.

TCD
8, 2831–2866, 2014

Krautblatter, M., Huggel, C., Deline, P., and Hasler, A.: Research perspectives on unstable high-Alpine bedrock permafrost: measurement, modelling and process understanding, Permafrost Periglac., 23, 80–88, doi:10.1002/ppp.740, 2011.
Juliussen, H. and Humlum, O.: Towards a TTOP ground temperature model for mountainous terrain in central-eastern Norway, Permafrost Periglac., 18, 161–184, doi:10.1002/ppp.586, 2007.
Leloup, P. H., Arnaud, N., Sobel, E. R., and Lacassin, R.: Alpine thermal and structural evolution of the highest external crystalline massif: the Mont Blanc, Tectonics, 24, TC4002, doi:10.1029/2004TC001676, 2005.
Le Roy, M.: Reconstitution des fluctuations glaciaires holocènes dans les Alpes occidentales, Thèse de Doctorat de Géographie, Université de Savoie, Le Bourget du Lac, 344 pp., 2012.
Luetschg, M., Lehning, M., and Haeberli, W.: A sensitivity study of factors influencing warm/thin permafrost in the Swiss Alps, J. Glaciol., 54, 696–704, 2008.
Noetzli, J., Gruber, S., Kohl, T., Salzmann, N., and Haeberli, W.: Three-dimensional distribution and evolution of permafrost temperatures in idealized high-mountain topography, J. Geophys. Res.-Earth, 112, F02S13, doi:10.1029/2006JF000545, 2007.
Noetzli, J., Ravanel L., and Deline P.: Combining measurements and modelling to describe the permafrost conditions at the Aiguille du Midi (3842 m a.s.l., Mont Blanc Massif), The Cryosphere, in preparation, 2014.
PERMOS: Permafrost in Switzerland 2002/2003 and 2003/2004, in: Glaciological Report (Permafrost) No. 4/5, edited by: Vonder Mühll, D., The Cryospheric Commission of the Swiss Academy of Sciences, Zürich, 121 pp., 2007.
PERMOS: Permafrost in Switzerland 2008/2009 and 2009/2010, in: Glaciological Report (Permafrost) No. 10/11, edited by: Noetzli, J., The Cryospheric Commission of the Swiss Academy of Sciences, Zürich, 95 pp., 2013.
Pogliotti, P.: Influence of Snow Cover on MAGST over Complex Morphologies in Mountain Permafrost Regions, Ph.D. thesis, Università degli Studi di Torino, Turin, 79 pp., 2011.
Pogliotti, P., Cremonese, E. M., di Cella, U., Gruber, S., and Giardino, M.: Thermal diffusivity variability in alpine permafrost rock walls, in: Proceedings of Ninth International Conference on Permafrost, Vol. 2, Institute of Northern Engineering, University of Alaska, Fairbanks, 1427–1432, 2008.

TCD
8, 2831–2866, 2014

Ravanel, L. and Deline, P.: Climate influence on rockfalls in high-Alpine steep rock walls: the north side of the Aiguilles de Chamonix (Mont Blanc massif) since the end of the "Little Ice Age", The Holocene, 21, 357–365, doi:10.1177/0959683610374887, 2010.

Ravanel, L., Allignol, F., Deline, P., Gruber, S., and Ravello, M.: Rock falls in the Mont Blanc Massif in 2007 and 2008, Landslides, 7, 493–501, 2010.

Ravanel, L., Deline, P., Lambiel, C., and Vincent C.: Intability of a high Alpine rock ridge: the lower Arête des Cosmiques, Mont Blanc massif, France, Geogr. Ann. A, 95, 51–66, doi:10.1111/geoa.12000, 2012.

Smith, M. W. and Riseborough, D. W.: Permafrost monitoring and detection of climate change, Permafrost Periglac., 7, 301–309, doi:10.1002/(SICI)1099-1530(199610)7:4<301::AID-PPP231>3.0.CO;2-R, 1996.

Smith, M. W. and Riseborough, D. W.: Climate and the limits of permafrost: a zonal analysis, Permafrost Periglac., 13, 1–15, doi:10.1002/ppp.410, 2002.

Williams, P. J. and Smith, M. W.: The Frozen Earth, 1st Edn., Studies in Polar Research, Cambridge University Press, Cambridge, 306 pp., 1989.

TCD
8, 2831–2866, 2014

Table 1. Instrument positions.

Site Code	Elevation [m a.s.l.]	Aspect [°]	Slope [°]	Sensor depths [m]
BH_S	3753	135	55	0.14, 0.34, 0.74, 1.04, 1.34, 1.64, 2.14, 2.64, 3.64, 4.64, 6.64, 8.64, 9.64
BH_N	3738	345	90	0.3, 0.5, 0.7, 0.9, 1.1, 1.4, 1.7, 2, 2.5, 3, 4, 5, 7, 9, 10
BH_E	3745	50	65	0.3, 0.5, 0.7, 0.9, 1.1, 1.4, 1.7, 2, 2.5, 3, 4, 5, 7, 9, 10
W1	3825	270	80	0.1
S1	3820	140	74	0.1
N1	3820	354	84	0.1
E1	3823	124	60	0.1
N2	3820	334	80	0.03, 0.1, 0.3, 0.55
E2	3820	118	60	0.03, 0.1, 0.3, 0.55
S2	3815	160	85	0.03, 0.1, 0.3, 0.55
W2	3825	270	85	0.03, 0.1, 0.3, 0.55
S3	3820	158	70	0.03, 0.1, 0.3, 0.55
AT	3842	0	0	–

BH: borehole thermistor chains, x1 and x2: rock surface temperature loggers, AT: air temperature.

TCD
8, 2831–2866, 2014

Table 2. Data availability after gap filling.

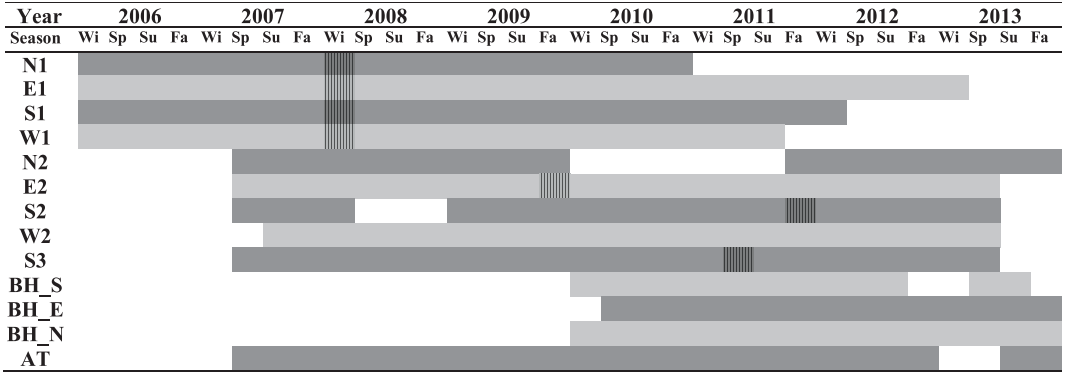

Wi: December, January, February; Sp: March, April, May; Su: June, July, August; Fa: September, October, November.
Striped sections indicate where gaps < 1.5 month have been filled in order to calculate annual means but seasonal means were not calculated for the seasons in question.

TCD
8, 2831–2866, 2014

Table 3. Borehole and air temperature records.

Year	BH_E			BH_S			BH_N		
	ALT [m]	Max. ALT [dd mm]	$MART_{10m}$ [°C]	ALT [m]	Max. ALT [dd mm]	$MART_{10m}$ [°C]	ALT [m]	Max. ALT [dd mm]	$MART_{10m}$ [°C]
2010	3.1	27 Jul	–	5.2	23 Oct	−1.4	1.8	28 Aug	−4.7
2011	2.7	30 Aug	−3.8	5.9	22 Oct	−1.5	2.3	18 Sep	−4.6
2012	3.3	26 Aug	−3.6	–	–	–	2.5	26 Aug	−4.3
2013	3.4	08 Sep	−3.6	5.8	30 Sep	–	2.2	25 Aug	−4.5

ALT: Active Layer Thickness.
$MART_{10m}$: Mean Annual Rock Temperature at 10 m deep.

TCD
8, 2831–2866, 2014

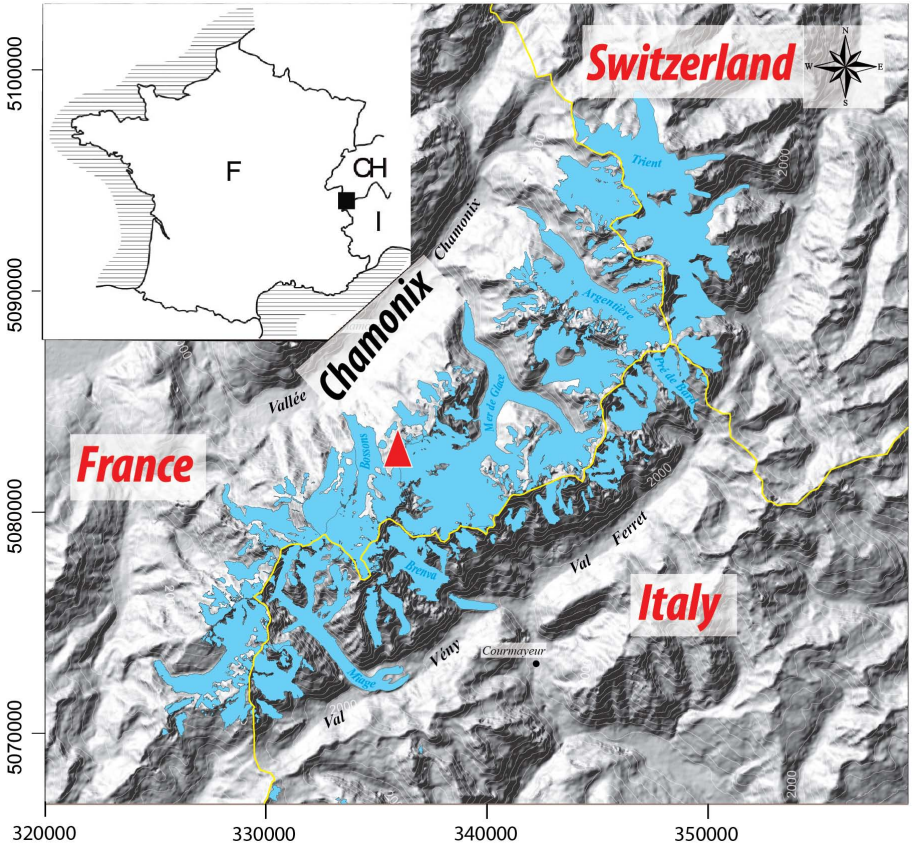

Figure 1. Location of the Mont Blanc Massif and the Aiguille du Midi (red triangle) (modified from Le Roy, 2012).

TCD
8, 2831–2866, 2014

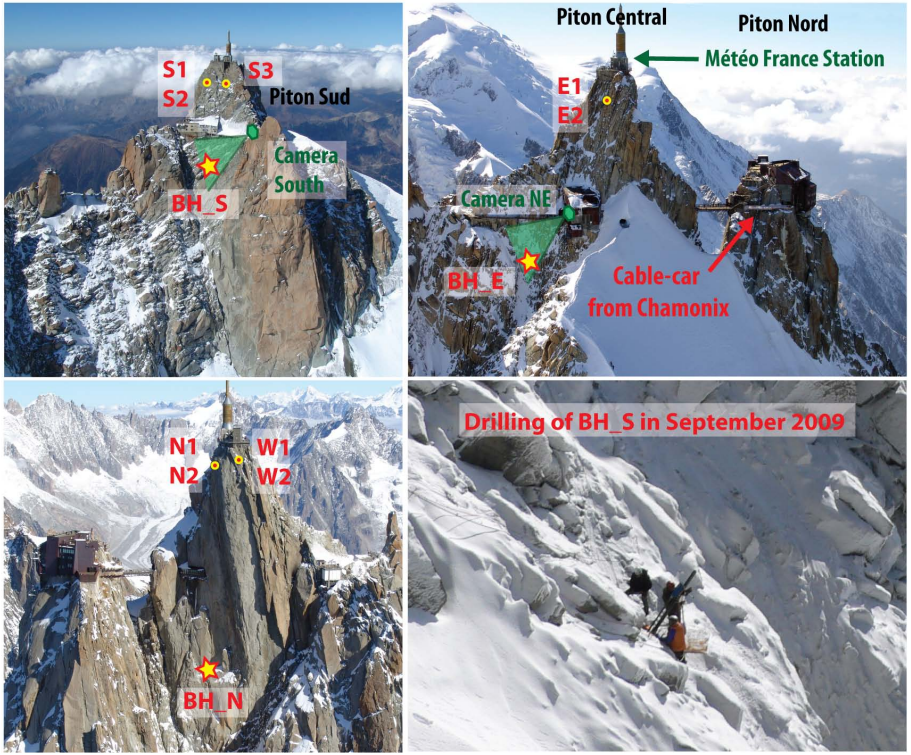

Figure 2. The Aiguille du Midi with camera, RST, and BH logger locations. Pictures: S. Gruber (top left and right, bottom left); P. Deline (bottom right).

TCD
8, 2831–2866, 2014

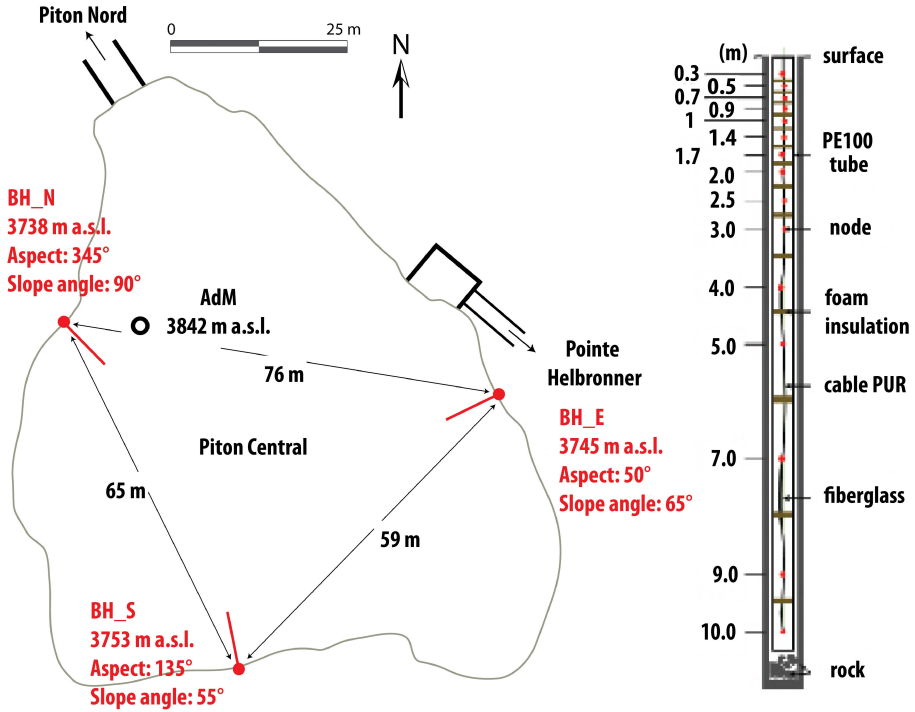

Figure 3. Borehole positions and components. Left: Horizontal cross-section through the AdM's Piton Central. Borehole positions are marked in red. Right: 10 m-long, 15 node thermistor chain installed in the boreholes.

TCD
8, 2831–2866, 2014

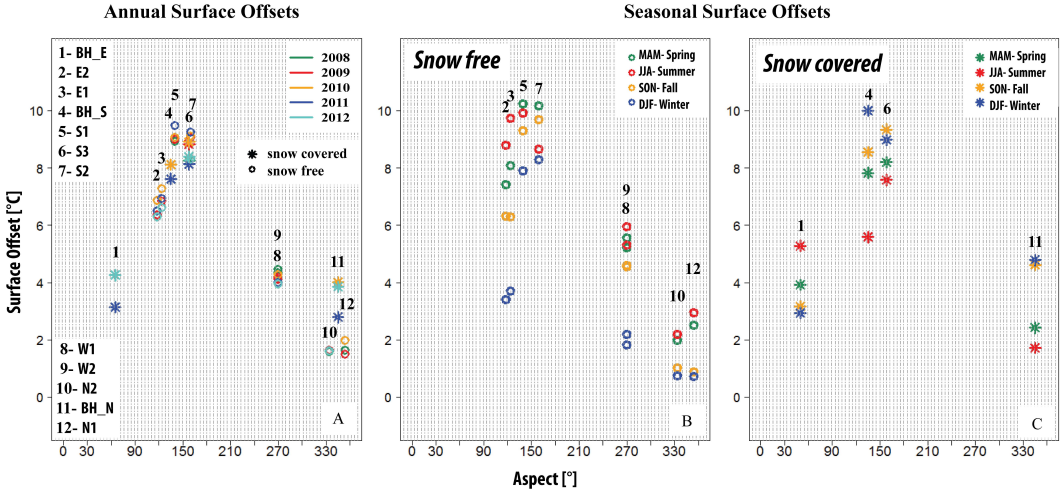

Figure 4. Annual and Seasonal Surface Offsets calculated from sensors at 0.3 m deep. ASOs are shown for all the available years. SSOs are the mean values for the available seasons for each logger listed in Table 2.

TCD
8, 2831–2866, 2014

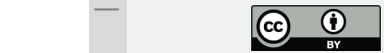

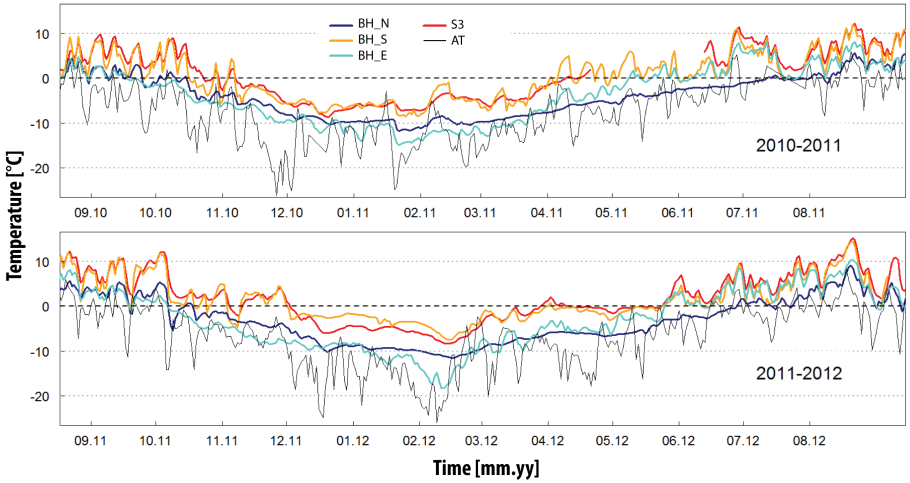

Figure 5. Daily temperature records at 0.3 m deep for snow-covered sensors for the 2010–2011 and 2011–2012 hydrological years.

TCD
8, 2831–2866, 2014

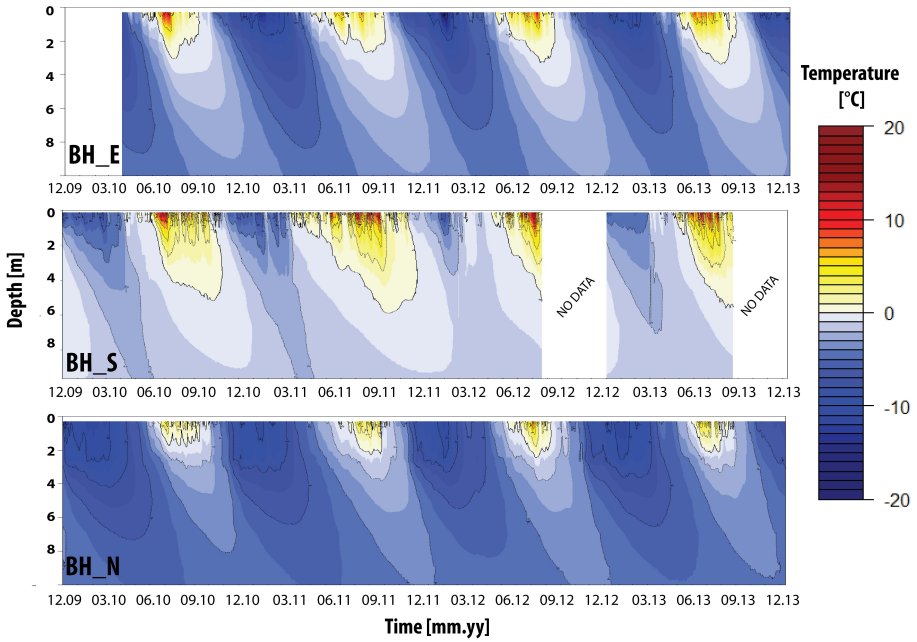

Figure 6. Daily temperature records in the AdM boreholes from December 2009 to January 2014.

TCD
8, 2831–2866, 2014

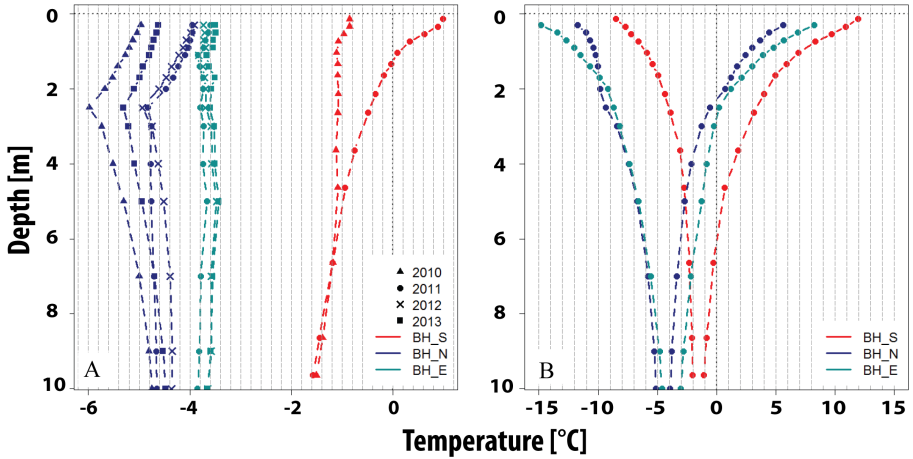

Figure 7. Mean $T(z)$ profiles **(A)** and 2011 temperature envelopes **(B)** of the AdM boreholes.

TCD
8, 2831–2866, 2014

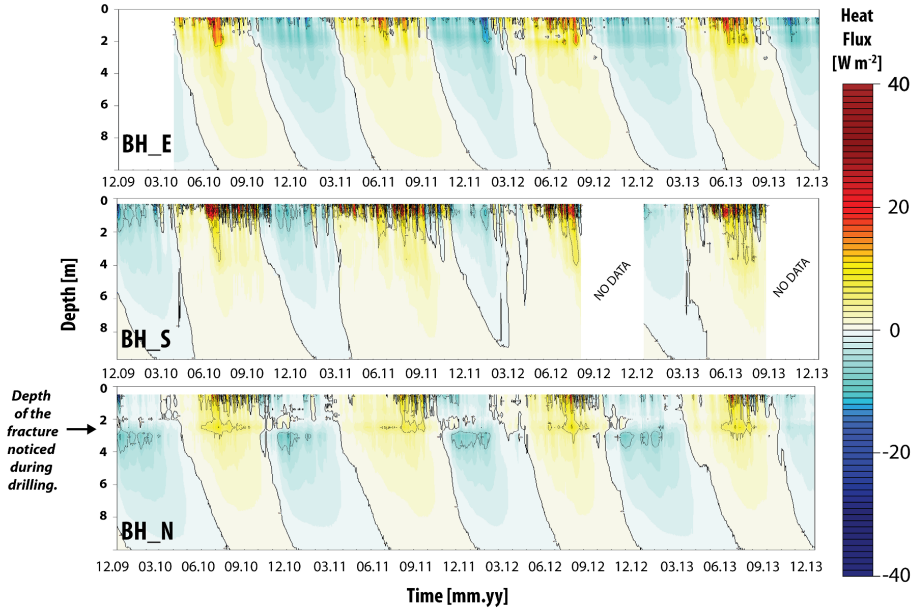

Figure 8. Daily heat flux [W m^{-2}] calculated from boreholes from December 2009 to January 2014.

TCD
8, 2831–2866, 2014